

# Electronic properties of DNA: structural and chemical influence on the quest for high conductance and charge transfer

R. G. Endres, D. L. Cox, R. R. P. Singh

*Department of Physics, University of California, Davis, CA 95616*

(Dated: November 20, 2018)

Motivated by the wide ranging experimental results on the conductivity of DNA, we have investigated extraordinary configurations and chemical environments in which DNA might become a true molecular wire, particularly from enhanced electronic overlaps or from small activation energies. In particular, we examine A- vs B-DNA, the ribbon-like structures proposed to arise from molecular stretching, the potential role of counterions in hole doping the DNA orbitals, the possibility of backbone conduction, and the effects of water. We find that small activation gaps observed in conductivity experiments may arise in the presence of water and counter ions. We further discuss the role of harmonic vibration and twisting motion on electron tight binding matrix elements using *ab initio* density functional theory and model Koster-Slater theory calculations. We find that partial cancellation between  $pp\sigma$  and  $pp\pi$  interaction of  $p_z$  orbitals on adjacent base pairs, along with destructive interference of phase factors are needed to explain the weak conductance of A-DNA. Our results lead also to a physical interpretation of the angular dependence of inter-base pair tight binding matrix elements. Furthermore, we estimate Franck-Condon factors, reorganization energies and nuclear frequencies essential for charge transfer rates, and find our estimated hole transfer rates between base pairs to be in excellent agreement with recent picosecond dynamics data.

## I. INTRODUCTION

In addition to DNA's fundamental role in genetics, it is now also a potential candidate for nano-electronic devices. The highly specific binding between single strands of DNA and its self-assembly property open a whole new approach to single-molecule electronics. However, its intrinsic conductance properties remain highly controversial. As early as 1962, Eley and Spivey suggested that  $\pi-\pi$  interactions of stacked base pairs in double stranded DNA could lead to conducting behavior[1]. Recently, there have been several experimental studies of the DNA conductance, leading to a variety of results. These have ranged from wide-gap insulating behavior to proximity induced superconductivity.

Although double stranded DNA has similarities to van der Waals stacked aromatic conducting crystals (*e.g.* the DNA base pair spacing is similar to the preferred axis lattice spacing of aromatic crystals) it also has essential differences from these and conventional conductors. Unlike crystals, the DNA is not a periodic system. The largest ionization potential difference between two isolated bases is about 0.6 eV between guanine and thymine which exceeds the estimated electronic coupling between base pairs. In addition, DNA's environment, *e.g.* its dynamical interaction with water and counterions, can have a substantial impact on its conductivity. From molecular dynamics simulations, the average displacement of a base pair in DNA is about  $0.3 - 0.4\text{\AA}$  [2] which is a tenth of the Watson-Crick spacing and an order of magnitude higher than in crystals at room temperature. All these properties make DNA a highly dynamic system and it remains unclear how well traditional concepts from solid state physics can describe it.

DNA has recently been the object of numerous single molecule studies to ascertain its conducting properties

directly. Results have varied dramatically, from finding a fully localized insulator[3], a wide gap semiconductor with coherent extended states[4], a metal at room temperature with ohmic current voltage characteristics and a conductance comparable to doped polyacetylene[5], and, most surprisingly, a proximity effect superconductor at very low temperatures[6]. Recently, self-assembled networks of DNA have been developed with quite reasonable conductance properties over distance scales of 50 nm or less, and high conductance induced by chemical or gated doping[7, 8]; these networks can be used to make transistor devices. Indeed, a single molecule DNA FET (field-effect transistor) has recently been constructed[8]. Motivated by these wide ranging experimental results on the conductivity of DNA, we have embarked on a theoretical effort to ascertain what conditions might induce such remarkable behavior. Our focus here is to examine whether any likely DNA-structures or environments can yield reduced activation gaps to conduction or enhanced electronic overlaps. In particular (sec. II), we have studied a hypothetical stretched ribbon structure, A, and B-form DNA, and the effects of counterions (especially sodium and magnesium) with and without water.

We have used a combination of fully *ab initio* density functional theory (DFT) code (SIESTA[9]), and a parameterized Hückel-Slater-Koster[10, 11] modeling using only atomic  $p_z$  orbitals ( $z$  the long axis of the molecule) of the bases.

We have been unsuccessful in identifying structural motifs that might engender metallic conductance in DNA, but we give an explanation why DNA in the A-form provides less effective electronic coupling along the helical axis than B-DNA. While direct matrix elements between two highest occupied molecular orbitals (HOMOs) or lowest unoccupied molecular orbitals (LUMOs) for model A-(B-)DNA are of order 0.01 eV (0.1 eV), indi-

vidual matrix elements between  $p_z$  orbitals on well contacted atoms in adjacent base pairs can generally exceed 1 eV.

We also demonstrate the possibility of small activation gaps of order  $k_B T$  with a first principles study of 4 base pair long B-DNA. We discuss the cases of sodium and magnesium counterions, with (wet DNA) or without water (dry DNA).

We have also studied the influence of longitudinal and torsional vibrations upon the electronic structure of DNA (sec. III), and estimated reorganization energies, Franck-Condon factors, and charge transfer rates between adjacent bases (sec.IV). We find good agreement between our estimated rates and recent experimental data[12] assuming that torsional (twist) vibrations limit the charge transfer most significantly. Finally, we conclude in section V. Some of the mathematical details can be found in appendix A.

## II. THEORETICAL SEARCH FOR HIGH CONDUCTANCE DNA

### A. Structural influence

In this section we demonstrate that the electronic coupling between base pairs is highly sensitive to the DNA-structure and thus to the influence of its environment, which can modify the structure.

In biological situations, there are several double helical conformations of DNA depending on the humidity and salt concentration. We consider the A- and B-forms. The B-form predominantly occurs *in vivo*, has a unit cell of 10 base pairs (neglecting sequence effects), a helical rise of about  $3.375\text{\AA}$  per base pair, and a twist angle between adjacent base pairs on average of  $36.0^\circ$  [13]. Since the base pairs are approximately perpendicular to the helical axis, the base pair separation is close to the helical rise. The A-form exists at low humidity in the presence of some salts. The double helix is relaxed to 11 base pairs in a unit cell exposing more of the hydrophobic core of base pairs and portions of the sugar units of the backbone. The helical rise and base pair separation are  $2.56\text{\AA}$  and  $2.425\text{\AA}$ , respectively. The twist angle is only  $32.7^\circ$ [14].

There are also other known conformations. In order to obtain straight DNA molecules for conductivity measurements, one often uses a technique called molecular combing [15]. When a DNA molecule is anchored at one end on a hydrophobic surface like polystyrene, a receding meniscus can stretch DNA by a factor of 1.7, or if grafted at both ends to the surface even by a factor as large as 2.1. The capillary forces are typically  $> 160pN$  and can become as large as  $500pN$  which results in breaking of the molecule. The stretching has been theoretically examined with molecular dynamics simulations using classical force fields [16]. Since the phosphate-phosphate distance along the backbone is about  $7\text{\AA}$  and the base pair separation in B-DNA is about  $3.4\text{\AA}$ , stretching by a factor

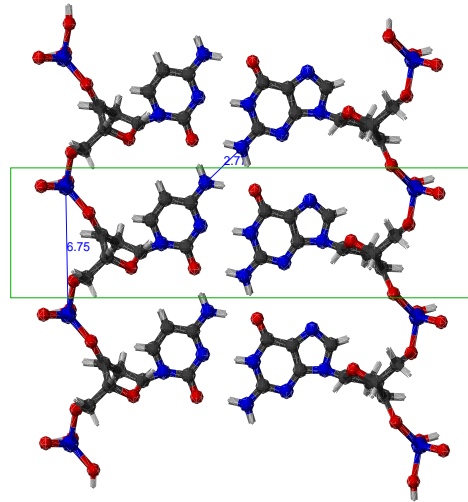


FIG. 1: Ideal 2-dimensional ribbon structure for DNA stretched by a factor of 2. The box indicates the unit cell of height  $6.75\text{\AA}$ . There are only very few good electronic contacts.

of 2 can, in principle, lead to a complete unwinding of the double helix. Since just stretching would weaken the inter base pair electronic coupling, we examine the possibility of base pairs which lie in the plane of the backbone strands (fig.1). In this case, the base pairs can come close again and the kinetic energy of the  $\pi$  electrons can in principle be lowered if there was decent  $pp\pi$  overlap between the  $p_z$  atomic orbitals at the closest contacts (with the z-axis now perpendicular to the ribbon). Ribbon-like structures are indeed found by K. M. Kosikov *et al* [16], e.g. the structures  $A_1$  or  $B_1$ , by using a classical force field.

### B. *Ab initio* estimates of electronic couplings

In order to get a realistic picture of the electronic coupling strength between two base pairs, the smallest structural unit through which charge has to go, we use the DFT code SIESTA [9]. Since its aim is efficiency and large systems, it uses Troullier-Martins norm-conserving pseudo potentials[17] in the Kleinman-Bylander form[18], and a basis set of numerical atomic orbitals using the method by Sankey and Niklewski[19]. We used a double- $\zeta$  basis set with polarization orbitals (DZP), the largest basis within SIESTA, and the generalized gradient approximation (GGA) for the exchange-correlation energy functional in the version by Perdew, Burke and Ernzerhof[20]. The structures for B and A-DNA were obtained from x-ray diffraction data ([13] and [14], respectively). Since the hydrogen atoms were missing in the A-DNA structural data, they were added and

relaxed with the conjugate gradient method. The ideal 2-dimensional ribbon structure of figure 1 was created artificially in order to get most effective  $pp\pi$  overlap and a small unit cell containing only a single base pair. As for the 2 base pair calculations, only methylated[21] base pairs without the backbone were used for simplicity.

Consider two molecular orbitals (MOs),  $\alpha$  from base pair 1, and  $\beta$  from base pair 2.  $\alpha, \beta$  are eigenstates from SIESTA for individual base pairs. They can be expanded in terms of the original atomic orbitals of SIESTA, e.g.  $|\alpha\rangle = \sum_{i=1}^{N_\alpha} c_i^\alpha |ao\rangle_i$  with  $N_\alpha$  being the dimension of the base pair 1, and  $c_i^\alpha$  and  $|ao\rangle_i$  the LCAO (linear combination of atomic orbitals) coefficients and atomic orbital basis states, respectively.

The electronic coupling  $t_{\alpha\beta}$  between states  $\alpha$  and  $\beta$  can be computed as follows using formulas for non-orthogonal states[22], *viz*

$$t_{\alpha\beta} = [t'_{\alpha\beta} - 0.5(t'_{\alpha\alpha} + t'_{\beta\beta})S_{\alpha\beta}](1 - S_{\alpha\beta}^2)^{-1} \quad (1)$$

$$t'_{\gamma\delta} = \sum_{i=1}^{N_\gamma} \sum_{j=1}^{N_\delta} c_i^\gamma c_j^\delta H_{ij}^{\gamma\delta}, \quad S_{\alpha\beta} = \sum_{i=1}^{N_\alpha} \sum_{j=1}^{N_\beta} c_i^\alpha c_j^\beta S_{ij}^{\alpha\beta}, \quad (2)$$

where  $\gamma$  and  $\delta$  can take the values  $\alpha$  or  $\beta$  according to eq. 1. The total Hamiltonian  $H$  (overlap  $S$ ) matrix of the two base pair system with dimensions  $(N_\alpha + N_\beta) \times (N_\alpha + N_\beta)$  can be obtained from SIESTA. It can be thought of as consisting of two diagonal blocks  $H^{\alpha\alpha}$ ,  $H^{\beta\beta}$  ( $S^{\alpha\alpha}$ ,  $S^{\beta\beta}$ ) representing the intra-base pair couplings (overlaps) and one off-diagonal block  $H^{\alpha\beta}$  ( $S^{\alpha\beta}$ ) representing inter-base pair couplings (overlaps).

The values for the electronic couplings  $t_{\alpha\beta}$  between two HOMOs, as well as two LUMOs, are shown in table I. As for the B-form, they are in general small and in good agreement with earlier *ab initio* studies [25–27], but for A and ribbon form they are much smaller than for the B-form. For the ribbon structure (including the backbone), we also carried out a band structure calculation after fully relaxing the geometry. The bands were calculated at 30 k points in the long direction using a Brillouin zone sampling at 3 k points. There was no sign of dispersion in agreement with the weak electronic coupling. That is, once stretched the base pair states localize.

Thus, our conclusion is that dehydrating (A conformation) and stretching of DNA should lead to even more highly localized states and insulating behavior than in B-DNA. For the ribbon, the main reason is that there are only very few ( $\approx 3$ ) close contacts ( $\approx 2.7\text{\AA}$ ) between neighboring base pairs (see also figure 1). For A-DNA, the weak coupling might seem a bit surprising since the base pair separation is much smaller than in B-DNA, but it can be understood in terms of less effective stacking. This is explored in the next subsection.

### C. Slater-Koster modeling of coupling strength

In order to understand the results in the previous subsection more quantitatively, we have performed model

TABLE I: Transfer integrals in eV between HOMOs ( $t_H$ ) and LUMOs ( $t_L$ ) of two base pairs. The calculations are done with SIESTA and DZP basis set. The expression dimer always stands for a two base pair long DNA sequence, e.g. the GG dimer stands for 5'-GG-3' DNA.

| dimer                   | A-DNA   |         | B-DNA   |        |
|-------------------------|---------|---------|---------|--------|
|                         | $t_H$   | $t_L$   | $t_H$   | $t_L$  |
| GG                      | 0.0069  | -0.0006 | -0.1409 | 0.0525 |
| GG(2.425\AA)(ref. [23]) |         |         | -0.6922 | 0.2548 |
| GG(0.0°)(ref. [24])     |         |         | 0.2385  | 0.3233 |
| 5'-AG-3'                | -0.0153 | 0.0060  | -0.0710 | 0.1124 |
| 5'-GA-3'                | -0.0113 | -0.0010 | -0.1871 | 0.0472 |
| AA                      | 0.0310  | -0.0120 | -0.0695 | 0.1054 |
| Ribbon                  |         |         |         |        |
| GG                      | 0.0039  | 0.0083  |         |        |

calculations varying the angular and spatial separation of bases. These are more readily performed than full *ab initio* calculations and often provide more physical insight. We restrict ourself to just atomic  $p_z$  orbitals, where the  $z$  axis can be defined locally by the normal of the corresponding base. In this case, two  $p_z$  orbitals from different base pairs couple by  $pp\sigma$  and  $pp\pi$  interactions, which we model with semi-empirical Slater-Koster theory[10, 11]

$$V_{ppX} = \eta_{ppX} \frac{\hbar^2}{md_o^2} e^{-d/R_c}. \quad (3)$$

We note  $\eta_{pp\sigma} > 0$  and  $\eta_{pp\pi} < 0$ . Here,  $d$  and  $m$  are distance and electron mass, and  $(\hbar^2)/(md_o^2) = 7.62eV$ . The exponential distance cut-off  $R_c$  and  $\eta$  are parameters to be determined by matching to *ab initio* results as discussed below. The interatomic matrix element between two “parallel”  $p_z$  orbitals depicted in figure 2 is

$$\begin{aligned} E_{zz} &= \sin^2 \phi V_{pp\sigma} + \cos^2 \phi V_{pp\pi} \\ &= \frac{\hbar^2 e^{-d/R_c}}{md_o^2} \left[ (\eta_{pp\sigma} + |\eta_{pp\pi}|) \frac{z^2}{l^2 + z^2} - |\eta_{pp\pi}| \right], \end{aligned} \quad (4)$$

According to this formula, the combination of close base pair separation *and* poor contacts reduces the electronic coupling between base pairs, i.e. can lead to cancellation effects.

A general formula for non-parallel orbitals, which is used for all our following model calculations can be found in the Appendix, eq. (A3). The normal of each base is taken for the direction for all  $p_z$  orbitals within that base, and is obtained by fitting a plane to each single base whose coordinates were obtained from x-ray diffraction data for A and B-DNA. This formula constitutes a straightforward way to calculate inter - base pair couplings for a variety of spatial and angular separations.

The Slater-Koster parameters  $\eta_{pp\sigma}$ ,  $\eta_{pp\pi}$  and cut-off  $R_c$  were determined from fitting to DFT data as follows: Starting from the DZP basis of SIESTA, we first identify the  $2p_z$  orbitals. These are the first- $\zeta$  orbitals of

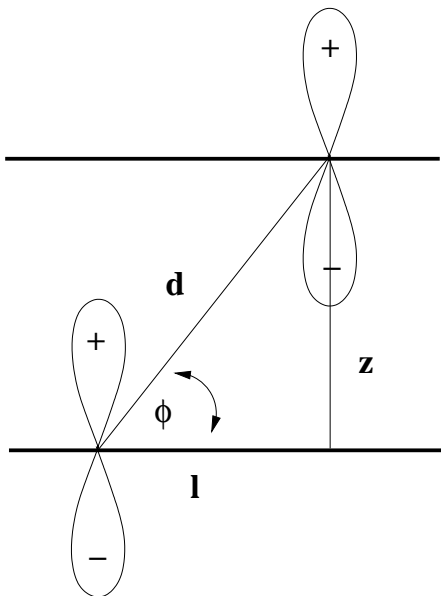


FIG. 2: Inter-atomic matrix elements from Slater-Koster theory: two atomic  $p_z$  orbitals on adjacent base pairs couple by positive  $pp\sigma$  and negative  $pp\pi$  interactions.

$p_z$  symmetry. (The second- $\zeta$  orbitals correspond to excited atomic states and have rather small contributions to the wavefunctions and matrix elements [ $\lesssim 20\%$ ].) We consider the reduced SIESTA Hamiltonian matrix in this basis, which has two diagonal blocks representing the on-site and intra-base pair couplings and one off-diagonal block representing inter-base pair couplings. The Slater-Koster matrix elements calculated with eq. (A3) are directly fitted to the off-diagonal block matrix elements. The fitting was done with simulated annealing, which gave better (and still physical) results than e.g. with the Powell algorithm[28]. Finally, since the DFT code uses a global  $z$ -axis along the helix which is different from the local  $z$ -axis due to an inclination and a propeller twist angle associated with each base, we turn to parallel reference base pairs for the fitting process. In the case of A-DNA we use two parallel  $G \cdot C$  base pairs with a separation of  $2.43\text{\AA}$ , while for B-DNA ones with a separation of  $3.34\text{\AA}$ . The fitted parameters are  $\eta_{pp\sigma} = 2.93$ ,  $\eta_{pp\pi} = -0.73$ ,  $R_c = 1.16\text{\AA}$  for A-DNA, and  $\eta_{pp\sigma} = 5.27$ ,  $\eta_{pp\pi} = -2.26$ ,  $R_c = 0.87\text{\AA}$  for B-DNA.

In order to further stress the difference between A and B-DNA, figure 3 shows a distribution of all possible  $p_z$  interatomic matrix elements between two  $G \cdot C$  base pairs in the A-form and in the B-form. Since guanine and cytosine have 11 and 8  $p_z$  orbitals, respectively there are a total of  $19 \times 19 = 361$  matrix elements. (Adenine and thymine have 10 and 8  $p_z$  orbitals respectively.) Figure 3 shows that there are more good contacts, e.g. twice as many above  $0.75$  eV, in the B-form than in A-form. Furthermore, there is a shift to (negative)  $pp\pi$  interaction

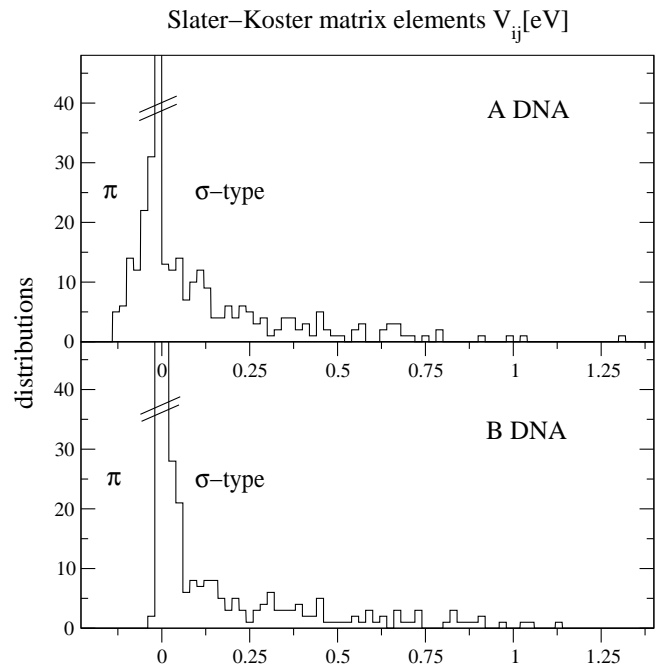


FIG. 3: Distribution of Slater-Koster inter-atomic matrix elements between  $p_z$  orbitals of two stacked  $G \cdot C$  base pairs. There are a total of 361 matrix elements. The smallest peak height corresponds to a single matrix element. Details about the distributions, mean: A 0.09, B 0.13; standard deviation: A 0.21, B 0.23; number of matrix elements above  $0.75\text{eV}$ : A 6, B 13.

in the A-form, although the single largest matrix element ( $\approx 1.3$  eV) arises in the A-form. This is presumably due to a single optimal contact at the shorter distance.

Table I shows the electronic couplings between specific MOs which correspond to HOMOs and LUMOs. A way to understand the smallness of  $t_{HOMO}$  ( $t_H$ ) and  $t_{LUMO}$  ( $t_L$ ) for A-DNA relative to B-DNA is to note that the distribution (fig. 3) is clearly more centered around zero in case of A-DNA, while for B-DNA it is more asymmetric with mostly positive matrix elements. The electronic coupling is a weighted average of these matrix elements with the weights being the product of two LCAO coefficients. It can be expected that the difference in the distributions leads to small electronic couplings for A-DNA.

Since A-DNA appears clearly insulating, as already indicated by the small bandwidth reported in ref. [3], we restrict ourselves to B-DNA in the subsequent sections.

#### D. Effect of counterions ions and water on electronic structure

DNA is a highly charged molecule which can only be stable if the negatively charged phosphate groups are neutralized by positive counterions or by polarized water molecules from a buffer solution. In order to measure its conductivity DNA has initially to be dried, normally by a

flowing  $N_2$  gas[7]. This can result in as few as 2 to 3 water molecules per nucleotide[29], which is not even high enough humidity to obtain the A-structure. In principle dried DNA can turn into a disordered structure[30] probably not suitable for charge transport through the base pairs at all. Evidence for that is found by STM images of dried DNA on mica, which shows a base pair separation of  $\sim 7.2\text{\AA}$  [31], and also by AFM images on  $SiO_2$  which show a DNA sample height of only 0.5 nm instead of the diameter 2nm of the usual double helix[32].

Different research groups in general work with different buffer solutions: activated (0.12 - 0.2 eV) hopping conductivity with an initial sodium ion buffer was observed by Kawai's group [8] using  $\mu\text{m}$  long poly(G)-poly(C)/poly(A)-poly(T) DNA, and by Rakitin *et al* [33], as well as Tran *et al* [29] using  $\lambda$ -DNA. On the other hand, proximity effect superconductivity was observed by Kasumov *et al* [6], who used a few 16- $\mu\text{m}$ -long  $\lambda$ -DNA molecules taken from a magnesium buffer solution.

Motivated by this, we have examined the effects of various counterions (protons, Na, Mg) and water on the electronic orbitals of DNA. We use a 4 base pair long 5'-GAAT-3' structure obtained from classical molecular dynamics (MD) with the AMBER 4.1 force field. The structure was taken from a snap shot of the Dickerson dodecamer with thousands of water molecules [2] and was provided to us by S. Dixit. For wet DNA we keep the first and second solvation shell ( $\sim 25$  water molecules per nucleotide), which corresponds to keeping all the water molecules within a 4.5  $\text{\AA}$  radius of the DNA atoms. Although B (wet) DNA exists only above 13 to 18 water molecules per nucleotide, we also examine completely dry DNA by removing all the water molecules but keeping the same B-DNA-structure. From our own experience with DFT calculations, DNA orbitals are generally rather localized on various groups like phosphate, sugar, counterions, and bases. Thus it might still be possible that this artificial dry DNA shows the correct order of energy levels and hence gives valuable information about activation gaps. The location of the counterions are kept the same as for wet DNA, i.e. some are further outside the DNA helix while others are at the phosphates or in the grooves. Counterion distributions are discussed in ref. [34]. For comparison we also considered protonated DNA of the same structure, since this is what theorists usually use for neutralized DNA. This has the big advantage of keeping the number of atoms small. The proton counterions are placed at the phosphates where they bind covalently. All other metal counterions and water molecules are removed.

We optimized the geometries with a few conjugate gradient steps (time consuming), but the forces still large (of order eV/ $\text{\AA}$ ). One can argue that this out-of-equilibrium structure might nevertheless resemble DNA in a solution at finite temperature where forces are always non-zero due to the motion of atoms and molecules. As a further check for dry DNA, we placed the metal ions at different locations and observed no principle changes occurred in

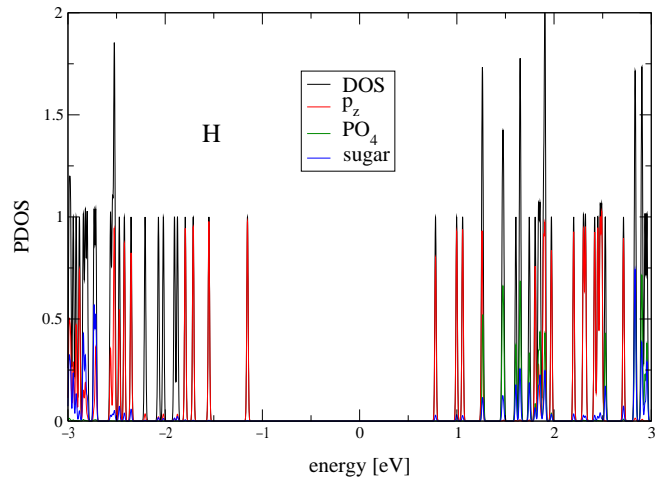


FIG. 4: PDOS of protonated 4 base pair long B-DNA; black: total DOS, red:  $p_z$  orbitals of atoms in base pairs, green: phosphate, blue: sugar. The Fermi energy is set to 0 eV.

the band structure or the Mulliken population[35] of the ions. For DNA we use a double- $\zeta$  basis set except for phosphorus, hydrogen involved in hydrogen bonding and the counterions for which we also include polarization orbitals. For the water molecules (more than 200) we only use a minimal, single- $\zeta$  (SZ) basis. The density of states (PDOS) is then projected onto atomic orbitals for energies around the Fermi energy  $\epsilon_F$  [36] to see which atomic orbitals can contribute to charge transport and what effects the counterions have on the eigenvalue spectrum.

The PDOS of the  $i$ th atomic basis orbital projected on the  $n$ th MO is

$$\rho_i^n(\epsilon) = \sum_j^{N_B} c_i^n c_j^n S_{ij} \delta(\epsilon - \epsilon_n), \quad (5)$$

where  $N_B$  is the dimension of the basis set,  $c_i^n, c_j^n$  are the LCAO coefficients and  $S_{ij}$  are the atomic overlap matrix elements. We project on the atomic  $p_z$  orbitals of the elements C, N and O of all the bases (resulting in  $\pi$  and  $\pi^*$  MOs), all orbitals of the five phosphate atoms, of the sugar atoms, counterions, and also whole water molecules.

The result for the protonated DNA is shown in figure 4. The atomic  $p_z$  orbitals (red) of the bases form an expected  $\pi - \pi^*$  gap of about 1.9 eV around  $\epsilon_F$  (set to zero). One has to keep in mind that DFT usually underestimates the gap in insulators by about 50 to 100%. The HOMO, mainly guanine, is about 0.4 eV higher than the next lower occupied MOs which are mostly adenine. The LUMO (cytosine) is about 0.2 eV lower than the next higher unoccupied MO (thymine). The occupied (unoccupied) phosphate states (green) and sugar states (blue) on the other hand are energetically lower (higher) than the  $\pi$  ( $\pi^*$ ) orbitals.

The results for sodium are shown in figure 5. Parts a) and b) contain the PDOS of wet DNA, i.e. part a) shows

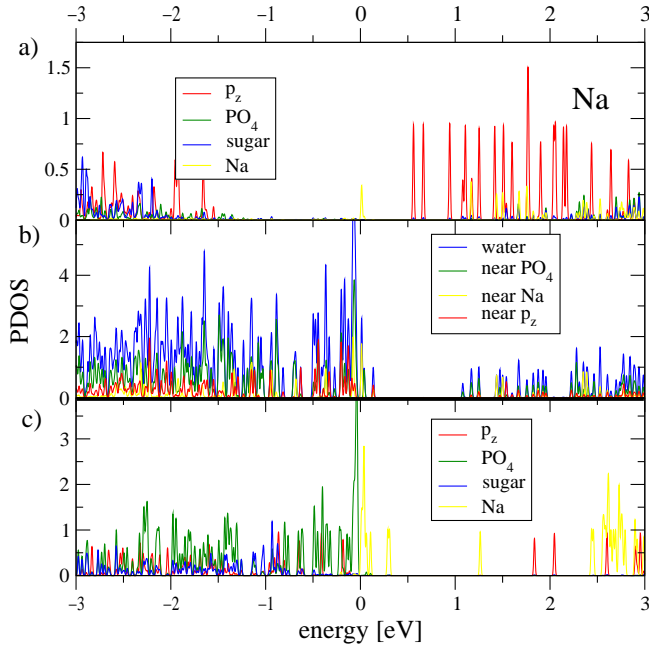


FIG. 5: Effects of sodium counterions and water on the molecular orbitals of 4 base pair long B-DNA. Part a) and b) show the PDOS of wet DNA; a) red:  $p_z$ , green: phosphate, blue: sugar, yellow: sodium; b) blue: all water molecules, green: water molecules near ( $< 3.5\text{\AA}$ ) phosphates, yellow: water molecules near sodium, red: water molecules near bases. In part c) all the water are removed (dry DNA).

the projection onto the bases ( $p_z$ ), phosphates, sugars, and sodium orbitals, while b) shows the projection onto water. In a) one can see a  $\pi - \pi^*$  gap of about 2.2 eV. It has slightly increased in the presence of water compared to protonated DNA. The highest  $\pi$  states around -1.6 eV (relative to  $\epsilon_F$ ) are mainly guanine, the next lower group of occupied states ( $\sim -1.9$  eV) are quite delocalized on several adenines with some guanine admixture. The first  $\pi^*$  state has mainly thymine character, the next higher also a little bit of cytosine. In the presence of water the  $\pi$  and  $\pi^*$  MOs seem to be more extended than in case of protonated DNA, where the MOs are more localized on individual bases.

Although the  $\pi - \pi^*$  gap is rather large, the real HOMO - LUMO gap is surprisingly small (54 meV). Electrons could possibly be excited from water levels below  $\epsilon_F$  into unoccupied water and sodium states. The presence of water and counterions might result in a weak conductance if a voltage is applied. Part b) of figure 5 separates the water PDOS (blue) into contributions coming from water molecules near the phosphates (green), near sodium (yellow), and near the bases (red). As one can see, the water states around  $\epsilon_F$  are mostly from water molecules near the sodium ions. The LUMO is a mixture of water and sodium. Furthermore, the negatively charged phosphates and positively charged sodiums are affecting the electronic structure of water drastically, since the several-eV large insulating gap of water is reduced to about 1

eV (0.7 eV in case of magnesium). A Mulliken population analysis of sodium reveals that sodium is on average a +0.88 charged ion. This is consistent with first principle studies of solvated metal ions, which indicate that solvated sodium is nearly a +1-ion almost independent of the water coordination number[37]. Regarding the sodium distribution, two sodiums are several  $\text{\AA}$  outside the DNA double helix, but the Mulliken population is hardly any different for these.

In order to see the effects of water on DNA more drastically, part c) of figure 5 shows the DOS of DNA with all the water molecules removed. Since the sodium ions (now only +0.66) are not directly located at the phosphates, they cannot screen their negative charges. Repulsive interactions likely between the oxygens of each phosphate group increase their energy (green) even beyond the  $\pi$  states (red). Although the  $\pi - \pi^*$  gap is about 2 eV, there are sodium states only 39 meV above the HOMO (phosphate). The PDOS is remarkably reproducible for different counterion configurations. One can speculate that due to the small electron excitation gap hole hopping through the backbone might be possible. Even if the B-DNA-structure is unstable under perfectly dry conditions, the quasi one-dimensional pathway for conduction through the backbone might still survive. One the other hand, the insulating sugars (blue) between the phosphates do not contribute much to the relevant states and constitute tunneling barriers.

For magnesium counterions, the result is shown in figure 6. Parts a) and b) contain the PDOS of wet DNA. Part a) shows the projection on DNA, while b) shows the projection onto water. In a) one can see a  $\pi - \pi^*$  gap of about 2.2 eV which is essentially the same as in the case of sodium. The highest  $\pi$  states at about -2.2 eV are a mixture of guanine and adenines, and 0.8 eV above an occupied adenine/thymine MO. The  $\pi - \pi^*$  gap is again much bigger than the real HOMO - LUMO gap, which is only 62 meV. Magnesium and water states below  $\epsilon_F$  could function as electron donors with electrons being excited into unoccupied  $\pi^*$  MOs leading to a possible electron conduction mechanism. From part b) of figure 6 one realizes however, that the water states right below  $\epsilon_F$  are not from water molecules in close proximity to the bases making the electron donation harder. The occupied water states from water near the bases are about 1 eV below the  $\pi^*$  MOs. A Mulliken population analysis of magnesium reveals that magnesium is not a +2-ion, but has a reduced +1.25 charge. One magnesium is more distant from the DNA molecule and is completely surrounded by water (7 water molecules within a radius of  $3\text{\AA}$ ). It has even a smaller (+1.0) charge. The smaller charge (less than +2) is again consistent with first principle studies of solvated metal ions, which indicate that magnesium solvated by 4 water molecules has a +1.1 charge, but less solvated magnesium has a larger positive charge closer to +1.7 [37].

Part c) of figure 6 shows the DOS of DNA with all the water molecules removed. Although the  $\pi - \pi^*$  gap

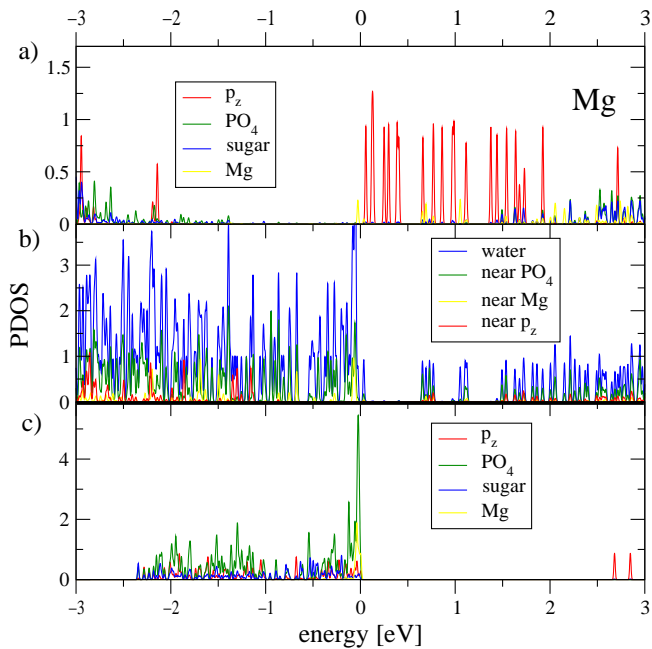


FIG. 6: Same as figure 5 except for magnesium counterions instead of sodium. Part c): there is a single magnesium state right above the Fermi energy ( $\epsilon_F = 0$ ).

is about 2.8 eV, there is a single magnesium state (not from the further outside one) only 11 meV above the HOMO (phosphate). The PDOS is again remarkably reproducible for different counterion configurations.

Finally, we try to give a possible explanation for the accumulation or pinning of phosphate states right below the metal states for dry DNA. Left unscreened, the occupied phosphate states will rise in energy due to repulsive interactions between negatively charged oxygens of a phosphate group. However, they cannot get higher than all the empty metal states. This is because if they were higher, the phosphates would dump electrons in the metal states and reduce their repulsive interactions. This would lower their energy, but if below the metal states, the phosphates would accept the electrons again, and the same process would repeat itself leading to the pinning-effect.

### III. DYNAMICAL INFLUENCE ON ELECTRONIC STRUCTURE

At finite temperature the base pairs of DNA will oscillate about their equilibrium positions. Within our model from section II C we are ultimately interested in the temperature dependence of the  $\pi - \pi^*$  band gap

$$\Delta_{\text{DNA}}(T) \approx \Delta_{\text{single bp}} - 2(\langle t_{\text{HOMO}} \rangle (T) + \langle t_{\text{LUMO}} \rangle (T)), \quad (6)$$

with  $\Delta_{\text{single bp}}$  being the temperature independent HOMO-LUMO gap of an isolated base pair, and  $\langle t \rangle (T)$

describing the temperature dependent average electronic coupling between adjacent base pairs. (In this model calculation, the  $\pi - \pi^*$  gap corresponds to the HOMO-LUMO gap, because we do not consider water here.) The goal is to understand the experiment by Porath *et al* who measured a strong increase of the voltage gap  $U_c$  (the minimal bias voltage above which conduction sets in) with temperature (2-4 eV per 300 K)[4]. In the experiment, short (30 base pair long) homogeneous poly(G)-poly(C) DNA molecules showed band-like semi-conducting behavior. In our calculation, we assume that displacements along the helical axis and the twisting motion are the most important degrees of freedom which affect the electronic coupling. For small changes in the variables, one can assume that these two degrees of freedom are independent.

Let  $\phi$  and  $u$  describe the deviations from equilibrium twist angle and base pair separation. Within our Koster-Slater-model in the CNDO (complete neglect of differential overlap) approximation, the transfer integral between two MOs of adjacent base pairs is given by eq. 1 with  $S_{12} = 0$ . (From our first principles calculations,  $0.001 \lesssim S_{12} \lesssim 0.01$ .) Thus we have  $t_{12} = \sum_{i,j} \tilde{H}_{ij}^{12} c_i^1 c_j^2$  where the LCAO coefficients are summed over each of the two base pairs and kept fixed for all  $\phi$  and  $u$ . They are given by the first- $\zeta$  orbitals of  $p_z$  symmetry from a single base pair DZP calculation, and are corrected by a factor  $\cos^{-1}\theta$  where  $\theta = 8.0^\circ$  is the angle between the local base normal and the helical axis. As noted earlier, the second- $\zeta$  orbitals yield  $\lesssim 20\%$  corrections to this. The matrix  $\tilde{H}^{12}$  is obtained as described in sec. II C and depends on  $\phi$  and  $u$  through the Slater-Koster form of the matrix elements. The tilde indicates that the reduced (first- $\zeta$ ) basis set was used. Since we calculate transfer integrals in CNDO, we do not need on-site energy matrices  $\tilde{H}^{11}$ ,  $\tilde{H}^{22}$  here. Nevertheless, these can be easily obtained in the same fashion. The resulting model can be used for very large scale quasi-self-consistent-field quantum calculations of long DNA sequences - similar to the one used for electron transfer rate calculations between various donors and acceptors in DNA[38].

In figures 7 and 8 we show the electronic coupling between the frontier orbitals as a function the variables  $\phi$  and  $u$ . One of them is held fixed at the equilibrium value, while the other one is varied. Consider first the variation with the angle  $\phi$  (fig. 7). At  $\phi = -36^\circ$ , i.e. when the two base pairs are aligned perfectly parallel, the coupling is maximal and positive. Let us focus on a GG dimer. At  $\phi = -36^\circ$ , there are 19 optimal contacts right on top of each other, and the transfer integral is approximately given by  $t \sim \sum_i \tilde{H}_{ii}^{12} (c_i)^2$  ( $c_i := c_i^1 = c_i^2$ ) where  $\tilde{H}_{ii}^{12} > 0$  is solely due to  $pp\sigma$  interaction. Note the interesting property that there are sign changes of  $t(\phi)$  with  $\phi$ . These provide a direct explanation for the local minima of  $|t|$  observed in earlier *ab initio* studies [25, 26]. In B-DNA, essentially all the interaction matrix elements ( $\tilde{H}_{ij}^{12} \gtrsim 0$ ) are positive ( $pp\sigma$  dominated), as can be seen in figure 3 and this is true for arbitrary twist angles  $\phi$ .

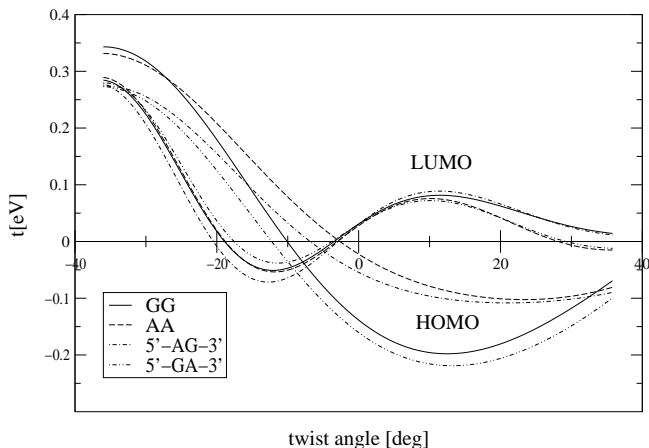


FIG. 7: Change of electronic coupling between frontier orbitals of two base pairs with relative twist angle  $\phi$  about the equilibrium position. The base pair separation is kept fixed at  $z = 3.375\text{\AA}$ .

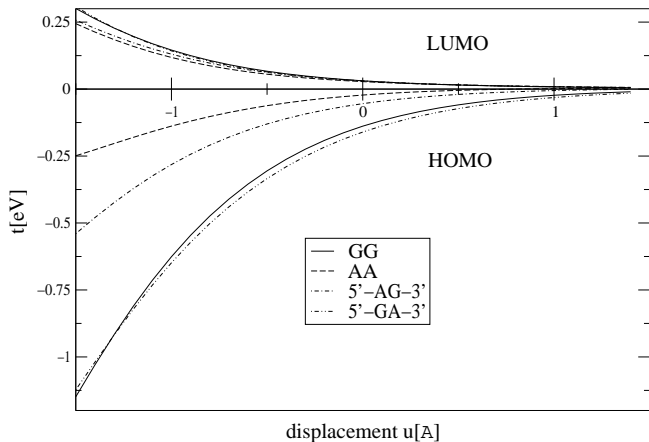


FIG. 8: Change of electronic coupling with relative displacement  $u$  about the equilibrium position. The twist angle is kept fixed at  $36.0^\circ$ .

Since for larger twist angles, i.e.  $\phi \approx 0$ , the transfer integral is approximately given by  $t \sim \sum_{i \neq j} \tilde{H}_{ij}^{12} c_i^1 c_j^2$ , the sign change of  $t$  can only come from the signs of the LCAO coefficients (phases of the  $p_z$  orbitals). This can lead to positive or negative  $t$ , or to a complete cancellation.

Coming back to the temperature dependence of  $t$  and the band gap, we assume classical harmonic potentials with spring constant  $K$  and shear constant  $S$  for each couple of base pairs. They can be estimated using the equi-partition theorem from classical statistical mechanics and estimates for the standard deviation from molec-

ular dynamics[2],

$$0.375^2 \text{\AA}^2 = \langle u^2 \rangle = \frac{k_B T}{K} \quad (7)$$

$$\rightarrow K = 0.184 \frac{eV}{\text{\AA}^2} = 294.8 \frac{pN}{\text{\AA}} \quad (8)$$

$$7.5^2 \text{deg}^2 = \langle \phi^2 \rangle = \frac{k_B T}{S} \quad (9)$$

$$\rightarrow S = 4.6 \cdot 10^{-4} \frac{eV}{\text{deg}^2}. \quad (10)$$

With these estimates for  $K$  and  $S$  the average electronic coupling can be calculated

$$\langle t \rangle (T) = \frac{\int dud\phi t(u, \phi) e^{-\frac{\beta}{2}(Ku^2 + S\phi^2)}}{\int dud\phi e^{-\frac{\beta}{2}(Ku^2 + S\phi^2)}}, \quad (11)$$

with  $\beta = 1/k_B T$ . The transfer integral only depends on the differences  $u = u_2 - u_1$  and  $\phi = \phi_2 - \phi_1$ , where  $u_i$  and  $\phi_i$  are the displacement and twist angle of the  $i$ th base pair. The results are shown in figures 9 and 10. Two things are remarkable about this result. First, the temperature dependence is very weak (a few meV change over hundreds of K). Second, harmonic displacement along the helical axis alone can lead to an increase in magnitude of the electronic coupling with increasing temperature  $T$ , while twisting motion on the other hand has the opposite effect leading to a cancellation.

This can be understood by looking at figures 7 and 8. Since  $t(\phi = 0)$  is closer to a local maximum (at least for HOMO states), a broadening of the gaussian distribution  $\sim e^{-\beta S \phi^2 / 2}$  with increasing temperature about  $\phi = 0$  will give more contribution from smaller  $t$ . On the other hand, a broadening of the distribution for  $u$  in the form  $e^{-\beta K u^2 / 2}$  will lead to more contributions from  $t$  with larger magnitude, since  $t(u)$  increases exponentially in magnitude when lowering  $u$ .

The weak temperature dependence of the electronic coupling, and hence of the band gap from eq. (6), are in strong contrast to the experiment by Porath and co-workers. It also calls to question the earlier analysis by Y. Berlin *et al* [39] who tried to explain the temperature dependence of the observed voltage gap  $U_c$  from a reduction of the bandwidth by only including torsional motion of base pairs. Our results imply a temperature independent  $U_c$  due to the cancellation of the two modes. The extremely strong increase of the gap with temperature could well be due to other effects[40]. The smallness of  $t$  does not allow much decrease of the bandwidth anyway.

#### IV. ESTIMATION OF PARAMETERS FOR CHARGE TRANSFER

Single electron or hole transfer is likely to be very sensitive to the actual motion of base pairs. Experimental evidence comes from the observation of two different time scales (5 and 75 ps) in charge transfer experiments[41].

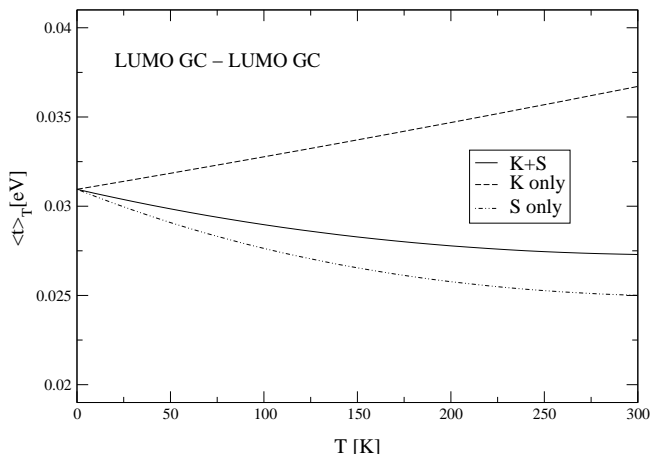


FIG. 9: Boltzmann averaged electronic coupling between LUMOs of two  $G \cdot C$  base pairs as a function of temperature  $T$ . The effects of a spring constant  $K$  and a shear constant  $S$  are shown.

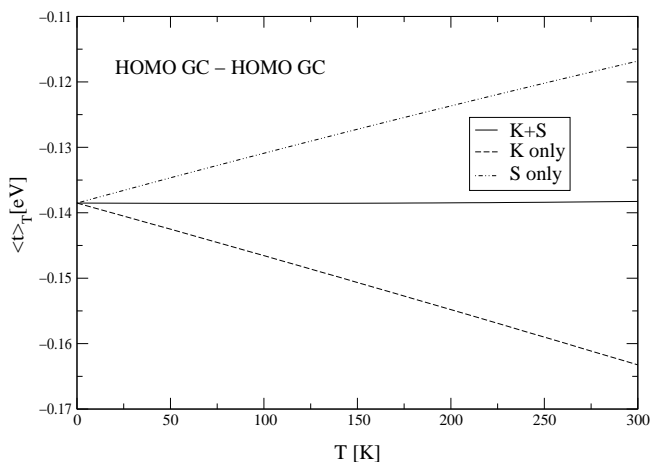


FIG. 10: Boltzmann averaged electronic coupling between HOMOs of two  $G \cdot C$  base pairs as a function of temperature  $T$ . The effects of a spring constant  $K$  and a shear constant  $S$  are shown.

The longer time stems presumably from a necessary re-orientation of base pairs in order to make charge transfer possible[41, 42]. Theoretically, torsional acoustic modes are indeed found to be extremely soft ( $\leq 20\text{cm}^{-1}$ ) [43] and hence slow, which is consistent with dynamic Stoke shifts in fluorescence spectra[44]. According to figure 7, the magnitude of the transfer integral oscillates between approximately 0 and 0.1-0.2 eV when one assumes a standard deviation of the twist angle of about  $10^\circ$  (actually more like  $7.5^\circ$ ). Under this assumption electron tunneling is possible on a time scale of the oscillation time  $T_S$  which can be estimated as  $T_S = 2\pi\sqrt{I/S}$ , where  $S$  is the shear constant and  $I = I_1 I_2 (I_1 + I_2)^{-1}$  the reduced moment of inertia of two base pairs.

More specifically, single charge transfer rates between two base pairs can be estimated from the classical Marcus

TABLE II: Inner reorganization energies  $E_{\lambda,i}$ , moments of inertia  $I$  and nuclear frequencies  $\nu_n$  of single base pairs. The calculations are done with SIESTA and DZP basis set.  $E_{\lambda,i}$  is determined by the energy difference of a hole/electron doped base pair between doped and undoped relaxed geometries. The moment of inertia is estimated with  $I = \sum m_i r_i^2$  where the sum is over all atoms of a base pair and  $r_i$  are measured from the helical axis of B-DNA. The nuclear frequencies are derived with  $E_{\lambda,i} = 2(\pi\nu)^2 \sum \mu_{i,i+1} u_{i,i+1}^2$  with  $\mu_{i,i+1}$  and  $u_{i,i+1}$  being the reduced mass and change in bond length of atoms  $i$  and neighbor  $i+1$  when comparing doped with undoped relaxed structures.

| $E_{\lambda,i}$ [eV]       | G·C  |          | A·T  |
|----------------------------|------|----------|------|
|                            | hole | electron |      |
|                            | 0.18 | 0.28     | 0.08 |
| $I[10^{-44}\text{kg m}^2]$ | 5.0  |          | 6.2  |
| $\nu_n[10^{13}\text{1/s}]$ | G·C  |          | A·T  |
|                            | hole | electron |      |
|                            | 3.97 | 5.09     | 3.64 |
|                            |      |          | 2.74 |

formula [45] (neglecting nuclear tunneling effects)

$$k_{CT} = \nu_n \kappa_{el} e^{-\beta\Delta E^*}, \quad (12)$$

where  $\nu_n$  and  $\Delta E^* = (E_\lambda + E_o)^2/(4E_\lambda)$  are the effective nuclear frequency and energy to reach the transition state, while  $\kappa_{el}$  describes the electronic transmission coefficient.  $E_\lambda$  is the total reorganization energy and  $E_o \leq 0$  is the reaction energy which is zero for charge transfer between homogeneous base pairs.

We expect the charge transfer between neighboring base pairs to be adiabatic, i.e.  $\kappa_{el} \approx 1$ , since the Landau-Zener probability  $P$  for crossing the surfaces at the transition state is close to unity with [46]

$$P = 1 - \exp(-2\pi\gamma) \quad (13)$$

$$\text{and } \gamma = \frac{t^2}{8h\nu_n\sqrt{\pi k_B T \Delta E^*}}. \quad (14)$$

This is because  $\gamma$  is large due to the relatively large transfer integral  $t$ . Inner shell reorganization energies and nuclear frequencies associated with adjusting the bonds between atoms of a single base pair can be calculated by the method of A. Klimkāns and S. Larsson described in [47]. The results are shown in table II, which also contains estimates for moments of inertia. The frequencies are quite similar to in-plane  $E_{2g}$  frequencies ( $4.8 \cdot 10^{13}\text{Hz}$ ) in graphite [48], and our calculated inner shell reorganization energies lie between those of benzene (0.26 eV) and anthracene (0.07 eV) [47], as one would expect from the number of aromatic rings involved. Since the total reorganization energy is estimated from experiments to be only about 0.4 eV [49] which is close to our values for the inner reorganization energies from table III, it suggests that the base pairs must be well protected by the double helix formation and solvation effects are minor. The small reorganization energies also contribute to the adiabaticity by increasing  $\gamma$  in equation 14.

TABLE III: Oscillation time of twisting motion  $T_S$ , total reorganization energy  $E_\lambda \approx \sum E_{\lambda,i}$ , Franck-Condon factor FC, and upper/lower limits of adiabatic charge transfer rates between two neighboring base pairs (bps). The rates are calculated with eq.(12) and data from table (II) in the normal regime. The upper limit corresponds to a nuclear frequency  $1/\nu = 1/\nu_n^1 + 1/\nu_n^2$ , the lower limit to  $\nu = 1/T_S$ .

| sequence(ref. [50])  |          | GG                  | AG(ref. [51])       | AA                  |
|----------------------|----------|---------------------|---------------------|---------------------|
| $T_S$ [ps]           |          | 2.02                | 2.13                | 2.25                |
| $E_\lambda$ [eV]     | hole     | 0.36                | 0.26                | 0.16                |
|                      | electron | 0.57                | 0.48                | 0.39                |
| FC (at 300K)         | hole     | 0.03                | 0.88                | 0.22                |
|                      | electron | 0.004               | 0.01                | 0.02                |
|                      | limit    |                     |                     |                     |
| $k_{hole}$ [1/s]     | upper    | $6.0 \cdot 10^{11}$ | $1.7 \cdot 10^{13}$ | $4.1 \cdot 10^{12}$ |
|                      | lower    | $1.5 \cdot 10^{10}$ | $4.1 \cdot 10^{11}$ | $9.9 \cdot 10^{10}$ |
| $k_{electron}$ [1/s] | upper    | $1.1 \cdot 10^{11}$ | $1.8 \cdot 10^{11}$ | $3.1 \cdot 10^{11}$ |
|                      | lower    | $2.1 \cdot 10^9$    | $4.7 \cdot 10^9$    | $1.0 \cdot 10^{10}$ |

Upper and lower bounds for the charge transfer rates between two base pairs are shown in table III. For the upper bound, we take  $\nu$  in equation (12) to be the inner base pair nuclear frequency, while for a lower bound we take it to be the base pair twist frequency. This slow process can be viewed as reaching an encounter complex with a frequency  $\nu = 1/T_S$ . We note the large Franck-Condon factor in table III for hole transfer between  $A \cdot T$  and  $G \cdot C$  (dimer AG). This is because this case is close to the so-called optimal electron transfer regime in which the reorganization energy (0.26 eV) is largely compensated by the reaction energy ( $0.20 \pm 0.05$  eV) [52] as estimated from analyzing electron transfer yield data. Note that this reaction energy is smaller than the difference of the bare oxidation potentials (0.4 – 0.5 eV) between isolated adenine and guanine bases in a polar solvent [53], in gas phase [54], or from *ab initio* calculations and Koopman's theorem[25, 55]. Furthermore, hole transfer is in most cases at least one order of magnitude faster and hence more efficient than electron transfer.

In order to compare with experiment we turn to (hole) transfer between initially excited 2-aminopurine (an isomer of adenine) and guanine [12]. The measured charge injection time of 10ps (corresponding to a rate of  $10^{11}$ 1/s) is surprisingly close to our lower bound value  $4.1 \cdot 10^{11}$ 1/s. Hence we speculate that the twisting motion of base pairs is rate limiting.

Another simple application of the 2 base pair charge transfer rates of table III is the hole hopping between homogeneous sequences, e.g.  $(A \cdot T)_N$ , when one assumes (biased) random walk as the underlying mechanism of the charge migration. In this case, the rate shows a weak algebraic distance dependence[56]  $k_{CT} \approx k_{HOP} N^{-\eta}$ , where  $N$  is the number intervening base pairs and  $1 \leq \eta \leq 2$ . Absolute rates can be predicted with our (lower bound) value  $k_{HOP} = 9.9 \cdot 10^{10}$ 1/s  $\approx 10^{11}$ 1/s. In order to compare with experiment, e.g. [57], one would have to include the

initial transfer from the donor to the bridge, as well as the final transfer from the bridge to the acceptor which leads to a further reduction of the rate. General formulas are provided in refs. [52, 56].

Finally, since charge transfer between adjacent base pairs is likely to be adiabatic, one should avoid including these when fitting to a diabatic charge transfer rate  $k_{CT} \sim \exp(-\beta R)$ . Including the adjacent base pair charge transfer in the fit leads to an under-estimation of  $\beta$ .

## V. CONCLUSIONS

In summary, we have studied the electronic properties of DNA from several perspectives. Our initial motivation was to come up with possible conditions which enhance the conductance of DNA. For example, we expected a stretched ribbon-like DNA to be a potential candidate for a molecular wire. Unfortunately, that has not turned out to be the case. Indeed, in the ribbon-like DNA, the base pair separation can become quite small. However, the  $pp\pi$  interaction appears not very effective as there are only very few good contacts. Using the *ab initio* code SIESTA we compared transfer integrals between base pairs of A, B and stretched DNA. Our calculations suggest that A-DNA and stretched, ribbon-like DNA should support electrical current even less than B-DNA.

On the other hand, a first principle study of 4 base pair long DNA in the B-form with different counterions (sodium, magnesium) under dry and wet ( $\sim 200$  water molecules) conditions shows the possibility of small activation gaps of order  $k_B T$ . Although the  $\pi - \pi^*$  gap is several eV large, a small gap is formed mainly by water and counterion states in the case of wet DNA, or by backbone and counterion states in the case of dry DNA. In the latter case, the backbone states rise in energy and lie higher than the occupied  $\pi$  MOs due to repulsive interactions of the negatively charged backbone. Since small activation gaps ( $\sim 0.1$ eV) are found experimentally for bundles[7, 33] or supercoiled DNA [8, 29] from a sodium buffer, this could be caused by residual water and condensed counterions providing an alternative pathway for charge hopping. To our knowledge, there is less experimental conductivity data available for DNA from a magnesium buffer. The most prominent case is the observed induced superconductivity [6] requiring truly extended metallic-like states. From our first principle studies of DNA with ions and water, we do notice some differences between magnesium and sodium ions. For wet DNA, electron excitation from occupied water and magnesium states into empty  $\pi^*$  states seems possible making electron conduction feasible. In addition, for dry DNA with magnesium ions, the activation gap between occupied backbone and unoccupied magnesium states is vanishingly small. In addition, there is a large DOS of phosphate states right below the Fermi energy available.

This pinning-effect opens the possibility of a pathway for hole hopping through the backbone.

In order to get a better microscopic understanding of the electronic coupling between adjacent base pairs and how it is affected by twisting and displacement motion, we developed a Hückel-Slater-Koster model with parameters obtained from *ab initio* calculations. We find that the transfer integral is constrained by a competition between  $pp\sigma$  and  $pp\pi$  interaction and interference by phase factors of atomic  $p_z$  orbitals. The latter effect also leads to sign changes in the transfer integrals as a function of the torsional angle not anticipated in previous studies.

Furthermore, the temperature dependence of the average transfer integral and band gap is expected to be weak: First, the electronic coupling is already weak anyway, and cannot be reduced much. Second, twisting and displacement motion of base pairs have cancelling contributions.

Next, we showed that charge transfer rates between adjacent base pairs are likely in the adiabatic limit. Thus, if one uses (modified) bases as donor and acceptor in charge transfer experiments, it is important to take this into account. When obtaining the decay length  $\beta$  of diabatic charge transfer from a fit to an experimental rate as a function of distance, the data point corresponding to the donor and acceptor next to each other should not be included in the fit.

We also calculated Franck-Condon factors, reorganization energies and nuclear frequencies to obtain absolute rate estimates. Furthermore, we suggest that the twisting motion might be rate limiting for hole transfer. Due to the adiabaticity of the two base pair rates, DNA might be a good medium for diffusive charge transport.

*Acknowledgements.* We would like to thank P. Ordejón, E. Artacho, D. Sánchez-Portal and J. M. Soler for providing us with their *ab initio* code SIESTA, as well as S. Dixit for providing us with the Dickerson dodecamer structure from classical molecular dynamics. We acknowledge helpful conversations with J.K. Barton, C.Y. Fong, and J. Jortner. This work was supported by the U.S. Department of Energy, Office of Basic Energy Sciences, Division of Materials Research, by a faculty seed

grant from the U.C. Davis office of research, by a collaborative seed grant from the Materials Research Institute of Lawrence Livermore National Laboratories, and by the National Science Foundation grant DMR-9986948.

## APPENDIX A: APPENDIX

In the following we derive a general formula for the calculation of interaction matrix elements between two atomic  $p_z$  orbitals belonging to adjacent base pairs. In general, the orbitals point in different directions, since the local z-axis is different for each base mainly due to a propeller twist angle, in case of A-DNA also because of a large inclination angle. We first expand the orbitals  $p_z, p'_z$  in a global coordinate system with the z-axis pointing in the direction of the helix

$$\begin{aligned} p_z &= \alpha \tilde{p}_x + \beta \tilde{p}_y + \gamma \tilde{p}_z \\ p'_z &= \alpha' \tilde{p}_x + \beta' \tilde{p}_y + \gamma' \tilde{p}_z, \end{aligned} \quad (\text{A1})$$

where the expansion coefficients are the direction cosines. If  $(l, m, n)$  is the unit vector pointing from one orbital to the other, the Slater-Koster relations [10]

$$\begin{aligned} E_{xx} &= l^2 V_{pp\sigma} + (1 - l^2) V_{pp\pi} \\ E_{yy} &= m^2 V_{pp\sigma} + (1 - m^2) V_{pp\pi} \\ E_{zz} &= n^2 V_{pp\sigma} + (1 - n^2) V_{pp\pi} \\ E_{xy} &= lm(V_{pp\sigma} - V_{pp\pi}) \\ E_{xz} &= ln(V_{pp\sigma} - V_{pp\pi}) \\ E_{yz} &= mn(V_{pp\sigma} - V_{pp\pi}) \end{aligned} \quad (\text{A2})$$

can be used to obtain the following formula for the interaction matrix element

$$\begin{aligned} V &= \alpha\alpha' E_{xx} + \beta\beta' E_{yy} + \gamma\gamma' E_{zz} \\ &+ (\alpha\beta' + \beta\alpha') E_{xy} + (\alpha\gamma' + \gamma\alpha') E_{xz} \\ &+ (\beta\gamma' + \gamma\beta') E_{yz}. \end{aligned} \quad (\text{A3})$$

The Slater-Koster matrix elements  $V_{pp\sigma}$  and  $V_{pp\pi}$  are given by eq. (3) and contain the distance dependence.

---

[1] D. D. Eley and D. I. Splivey, *Trans. Faraday Soc.*, **58**, 411 (1962)  
[2] M. A. Young, G. Ravishanker and D. L. Beveridge, *Biophys. J.*, **73**, 2313 (1997)  
[3] P. J. de Pablo *et al*, *Phys. Rev. Lett.* **85**, 4992 (2000)  
[4] D. Porath, A. Bezryadin, S. De Vries, and C. Decker, *Nature (London)* **403**, 635 (2000)  
[5] H. W. Fink and C. Schönberger, *Nature* **398**, 407 (1999).  
[6] A. Y. Kasumov *et al*, *Science* **291**, 280 (2001)  
[7] L. Cai, H. Tabata, and T. Kawai, *Appl. Phys. Lett.* **77**,

3105 (2000)  
[8] K. -H. Yoo *et al*, *Phys. Rev. Lett.* **87**, 1981 (2001)  
[9] D. Sánchez-Portal, P. Ordejón, E. Artacho, and J. M. Soler, *Int. J. Quantum Chem.* **65**, 453 (1997); E. Artacho, D. Sánchez-Portal, P. Ordejón, A. Garcia, and J. M. Soler, *Phys. Status Solidi (b)* **215**, 809 (1999); P. Ordejón, E. Artacho, J. M. Soler, *Phys. Rev. B* **53**, R10441 (1996)  
[10] J. C. Slater, G. F. Koster, *Phys. Rev.* **94**, 1498 (1954)  
[11] W. A. Harrison, *Electronic Structure and the Properties of Solids*, Dover Publications, Inc., New York, p.48,481

- (1989)
- [12] C. Wan, T. Fiebrig, O. Schiemann, J. K. Barton, A. H. Zewail, *Proc. Natl. Acad. Sci.* **97**, 14052 (2000)
- [13] R. Chandrasekaran and S. Arnott, *J. Biomol. Struct. Dynamics*, **13**, 1015 (1996)
- [14] S. Arnott and D. W. L. Hukins, *Biochem. Biophys. Res. Commun.*, **47**, 1504 (1972)
- [15] D. Bensimon, A. J. Simon, V. Croquette, A. Bensimon, *Phys. Rev. Lett.* **74**, 4754 (1995); J. F. Allemand *et al.*, *Biophys. J.*, **73**, 2064 (1997); I. Parra and B. Windle, *Nature Genetics*, **5**, 17 (1993); C. Bustamante, S. B. Smith, J. Liphardt, and D. Smith, *Curr. Opin. Struct. Biol.* **10**, 279 (2000)
- [16] A. Lebrun and R. Lavery, *Nucl. Acids Res.*, **24**, 2260 (1996); M. W. Konrad and J. I. Bolonick, *J. Am. Chem. Soc.*, **118**, 10989 (1996); K. M. Kosikov *et al.*, *J. Mol. Biol.*, **289**, 1301 (1999)
- [17] N. Troullier, J. L. Martins, *Phys. Rev. B* **43**, 1993 (1991)
- [18] L. Kleinman, D. M. Bylander, *Phys. Rev. Lett.* **48**, 1425 (1982)
- [19] O. F. Sankey, D. J. Niklewski, *Phys. Rev. B* **40**, 3979 (1989)
- [20] J. P. Perdew, K. Burke, M. Ernzerhof, *Phys. Rev. Lett.* **77**, 3865 (1996)
- [21] terminal CH<sub>3</sub> groups replace the backbone
- [22] M. D. Newton, *J. Phys. Chem.*, **90**, 3734 (1986)
- [23] Corresponds to perpendicular base pair separation of A-DNA which has a tilt angle of 20°. Note the huge difference to A-form GG.
- [24] Perfectly parallel aligned base pairs. Note the sign change compared to B-form GG at 36°.
- [25] H. Sugiyama and I. Saito, *J. Am. Chem. Soc.* **118**, 7063 (1996)
- [26] M. L. Zhang, M. S. Miao, V. E. van Doren, J. J. Ladik, J. W. J. Mintmire, *J. Chem. Phys.* **111**, 8696 (1999)
- [27] A. A. Voityuk, J. Jortner, M. Bixon, and N. Rösch, *J. Chem. Phys.* **114**, 5614 (2001)
- [28] [http://www.ulib.org/webRoot/Books/Numerical\\_Recipes/bookc.html](http://www.ulib.org/webRoot/Books/Numerical_Recipes/bookc.html)
- [29] P. Tran, B. Alavi, and G. Gruner, *Phys. Rev. Lett.* **85**, 1564 (2000)
- [30] A. J. Hopfinger, *Intermolecular interactions and bimolecular organization* (Wiley, New York, 1977) ch.7
- [31] L. Cai, H. Tabata and T. Kawai, *Nanotechnology* **12**, 211 (2001)
- [32] A. J. Storm *et al.*, *Appl. Phys. Lett.*, **79**, 3881 (2001)
- [33] A. Rakitin *et al.*, *Phys. Rev. Lett.* **86**, 3670 (2001)
- [34] M. A. Young, B. Jayaram, and D. L. Beveridge, *J. Am. Chem. Soc.* **119**, 59 (1997); A. P. Lyubartsev, A. Laaksonen, *J. Biomol. Struct. Dynamics* **16**, 579 (1998); Alexandre M. J. J. Bonvin, *Eur. Biophys. J.* **29**, 57 (2000); R. N. Barnett *et al.*, *Science* **294**, 567 (2001)
- [35] R. S. Mulliken, *J. Chem. Phys.* **23**, 1833 (1955)
- [36] To facilitate convergence, SIESTA can employ a finite temperature in the occupancy functions, which allows for a unique determination of the Fermi energy; for  $T = 0K$  this is of course indeterminate, and we have taken the Fermi energy at the midpoint of the HOMO-LUMO gap.
- [37] M. C. Vicens and G. E. López, *J. Comp. Chem.* **21**, 64 (2000)
- [38] S. Priyadarshy, S. M. Risser and D. N. Beratan, *J. Phys. Chem.* **100**, 17678 (1996)
- [39] Y. A. Berlin, A. L. Burin, and M. A. Ratner, *Superlattices Microstruct.* **28**, 241 (2000)
- [40] M. Hjort and S. Strafström, *Phys. Rev. Lett.* **87**, 228101/1-4 (2001)
- [41] C. Wan *et al.*, *Proc. Natl. Acad. Sci. USA* **96**, 6014 (1999)
- [42] R. Bruinsma, G. Gruner, M. R. D'Orsogna, J. Rudnick, *Phys. Rev. Lett.* **85**, 4393 (2000)
- [43] S. Cocco and R. Monasson, *J. Chem. Phys.* **112**, 10017 (2000)
- [44] E. Brauns *et al.*, *J. Am. Chem. Soc.* **121**, 11644 (1999)
- [45] R. A. Marcus and N. Sutin, *Biochim. Biophys. Acta* **811**, 265 (1985)
- [46] L. D. Landau, *Phys. Z. Sowjetunion* **1**, 88 (1932); **2**, 46 (1933); C. Zener, *Proc. R. Soc. London A* **137**, 696 (1932); **140**, 660 (1933)
- [47] A. Klimkäs and S. Larsson, *Chem. Phys.* **189**, 25 (1994)
- [48] C. T. Chan, K. M. Ho and W. A. Kamitakahara, *Phys. Rev. B* **36**, 3499 (1987)
- [49] A. Harriman, *Angew. Chem. Int. Ed. Engl.* **38**, 945 (1999)
- [50] Electron transfer actually involves the complementary bases C and T.
- [51] We used the following reaction energies: hole transfer between A and G,  $E_o = -0.2$  eV; electron transfer between T and C,  $E_o \approx 0$  eV.
- [52] M. Bixon and J. Jortner, *J. Am. Chem. Soc.* **123**, 12556 (2001)
- [53] C. A. M. Seidel, A. Schulz and M. H. M. Sauer, *J. Phys. Chem.* **100**, 5541 (1996); S. Steenken and S. V. Jovanovic, *J. Am. Chem. Soc.* **119**, 617 (1997)
- [54] V. M. Orlov, A. N. Smirnov and T. M. Varshavsky, *Tet. Lett.* **48**, 4377 (1976); S. G. Lias, J. E. Bartmess, J. F. Liebman, L. J. Holmes, R. D. Levin, W. G. Mallard, *J. Phys. Chem. Ref. Data* **17** (1988)
- [55] S. D. Wetmore, R. J. Boyd and L. A. Eriksson, *Chem. Phys. Lett.* **322**, 129 (2000)
- [56] J. Jortner, M. Bixon, T. Langenbacher and M. E. Michel-Beyerle, *Proc. Natl. Acad. Sci. USA* **95**, 12759 (1998)
- [57] F. D. Lewis *et al.*, *Science* **277**, 673 (1997)